CrystEngComm

Accepted Manuscript

ROYAL SOCIETY OF CHEMISTRY

www.rsc.org/crystengcomm

Simulating growth morphology of urea crystals from vapour and aqueous solution

M. K. Singh†
Laser Materials Development and Devices Division
Raja Ramanna Centre for Advanced Technology, Indore, India.
Fax: 91 731248 8650; Tel: 91 731248 8677;
†E-mail: mksingh@rrcat.gov.in.

Abstract

The molecular-scale understanding of the mechanism through which solvent interacts with the crystal surface during the crystal growth process is still a formidable challenge. The quantitative understanding at this end has a paramount interest in chemical and pharmaceutical industries in controlling the evolution of growth morphologies. Here we present a crystal growth model to elucidate the effect of internal and external growth parameters, solute, solvents and their corresponding concentrations to predict the growth morphology of crystalline urea from vapour and aqueous solution. The approach is based on details of thermodynamic and kinetic aspect of adsorption of solute and solvent molecules at crystal faces, thus, relating crystallographic information, different solid-liquid interfacial energetics and external growth parameters to rate of growth can be taken into account in a natural way. The binding energy of the solute molecules on the crystal surfaces is described by the molecular attachment energies which, in turn, depends on the molecular orientation and surface relaxation of the habit faces. Periodic first-principles method has been employed for accurate determination of solid-solid and solid-liquid energetics which are further utilized to calculate solvent-induced step energy and local dissolution enthalpy of solute molecules at various faces of the urea crystal. Our results show that the step energy decreases with increasing supersaturation and temperature. On the other hand, increase in supersaturation increases effective concentration and local dissolution enthalpy of the urea molecule in aqueous solution. The rate of growth of different faces of the urea crystal as a function of the driving force at various temperature have determined within the framework of the discussed model and the growth morphologies have been obtained. Our results show the appearance of block and needle-like habits of the urea crystals from vapour and aqueous solution, respectively, as functions of supersaturation and temperature which are in excellent agreement with the corresponding experimental observations.

1 Introduction

The molecular-scale understanding of the crystallization processes and the role played by solvent, tailor-made additive and growth environment is essential for a predictive design of the crystal growth experiments. A *priori* prediction of the progression of crystal morphologies requires accurate determination of various interactions occurring at crystal surfaces and growth expression relating kinetic and thermodynamic factors. The precise control of these parameters not only alter the properties, growth morphology and kinetics of the growing crystal, but the quantitative understanding at this end will eventually lead to an important intervention point for crystal engineering. During solvent-induced crystallization, ordering of the solvent molecules near crystal surface determines many important physical and chemical processes, such as crystal growth, wetting, lubrication and catalysis.[1-3] The surface structure of the crystal faces can vary from bulk terminated crystallographic structure and depends upon surface termination, the possible reconstruction and relaxation of the crystal surface. Likewise, the liquid structure near the interface may also differ from the bulk liquid structure because solvent molecules experience periodic potential of the crystal surface and expected to show more ordering than in the bulk liquid. The mechanism of action by which solid-liquid interface exerts its influence is still a matter of debate. There are two apparently contradicting suggestions that attempt to examine the effect of solvent on crystal growth. In the surface roughening hypothesis[4-8] the favourable interaction of solvent with the specific crystal faces leads to reduction of the interfacial surface tension. The consequence is a transition from a smooth to a rough interface and a resultant increase in the rate of growth of the affected faces. According to other hypothesis, the solvent exerts its effect by preferential adsorption at the growing crystal surfaces and inhibits the growth of specific faces,[9-12] since the solute molecules would be in competition with the solvent molecules for the growth sites. Thus, it is expected that the highly ordered solvent molecules near the interface alter the step energy and, thus, slow down the incorporation of the growth units into the crystal faces. It is because the attachment of solute molecules would require removal of the periodically adsorbed solvent molecules. The crystal faces whose rate of growth is inhibited become morphologically important whilst those that are growing relatively faster show a decrease in importance.

In many cases, little is known about the atomic structure of such interfacial layers, and therefore the correlation between macroscopic phenomena and molecular scale processes at the interface often remains speculative. To investigate the role of solid-liquid interface in actual processes obtaining detailed molecular-scale understanding of the interface is therefore of interest in determining the effects of solvent, impurity and surfactant on crystal growth morphology and bulk crystal structure.[9,13] The equilibrium form of the crystal can be constructed from a consideration of the surface free energies of the various crystallographic faces (*hkl*).[14] The thermodynamic morphology can readily be predicted,[15] but most particle shapes are difficult to predict because the particle morphologies are actually controlled by the kinetics and thermodynamic factors of the atomic growth processes. Many growth models have been proposed[16-18] to relate rate of growth to geometric or energetic characteristics of the surface, but these have met with limited success in predicting the observed crystal growth morphologies.

The prediction of the growth morphology of urea crystal from vapour and aqueous solution as a function of different growth parameters has been investigated in the present paper. Hartree-Fock (HF) and density functional methods (DFT) using hybrid exchange-correlation functional have been employed to compute solid-solid and solid-liquid interactions. The aqueous growth of urea has been chosen to study

the effect of solvent and other external parameters because the shape of urea crystal is known to change from block to needles like with large aspect ratio when the vapour medium is replaced by aqueous growth. To this end, the effect of internal and external growth parameters like molecular orientation, surface relaxation, supersaturation, temperature, solubility and the binding energies of solute and solvents to the crystal surfaces on the rate of growth has examined.

The rest of the paper is organized in the following manner. A brief discussion on the earlier approaches to model crystal growth morphology is presented in section 2. Section 3 outlines the methodology used to calculate different habit controlling energetics followed by a discussion on computational method in section 4. The results obtained from our calculations are discussed in section 5 and the paper is concluded in section 6.

2 Earlier Approaches to Model Crystal Growth Morphology

Before we discuss the method to study the role of solvent and other external factors affecting the rate of growth, we first discuss earlier approaches in order to place our work in proper perspective.

2.1 Predicting Crystal Morphology from Vapour

Initial attempts to predict the shapes of the crystal were made by Bravais (1866), Friedel (1907), and Donnay and Harker (1937).[16] In 1955, a significant contribution was made by Hartman and Perdok (HP)[17] and later modified by Hartman and Bennema,[18] who developed the idea of strong bond in their periodic bond chain (PBC) theory, connected nets, and roughening to predict external shape of crystal. A series of contributions by Hartman and Perdok provided the attachment energy (AE) model, which is useful in predicting the growth shape of crystal from vapour phase. The model was designed to realize the significance of intermolecular energies in morphology prediction. The development of the AE model was an important milestone in the prediction of crystal morphology. The AE model often makes good predictions for crystals that are grown from vapour.[17,18,19] In spite of great success, the model does not take into account of orientation of growth units (GUs) because the AE model is based on the assumption that a slab of thickness d_{hkl} attached to the face without considering the effect of molecular orientation of GUs on habit controlling energetic. The GU is the essential building block that transfers structural information from the solution/vapour to the crystal surface. Also, AE model can not be used to predict the growth shape of crystals that are obtained from solutions because the model does not include the effect of solvent and other external growth factors.

On the other hand, Clydesdale *et al*.[20] showed that, by using the crystal chemistry and molecular modelling procedures which can use to optimize the position and orientation of growth species on the host lattice, it is possible to simulate the vapour growth shape of crystals. Their approach can also use to model the effect of impurities on growth morphologies. Liu *et al.*[21] and Singh *et al.*[22] have studied the role of molecular orientation to predict growth shape of molecular crystals. Our results[22] show that, in the case of unit cell comprising more than one GU, the inclusion of molecular orientation and surface relaxation to AE model can significantly enhance the predictive power of attachment energy model. The consideration of molecular orientation to obtain habit controlling energetic is equally applicable to compute growth shape of molecular crystals from solutions.

2.2 Modelling Solvent-Induced Habit Modification

Next we describe the present status of our understanding on the mechanism of crystal growth and capability to predict crystal morphology. Solution growth technique is a convenient method which is widely used to grow large number of crystals. However, the computational complexity involved to predict the growth shape from solution is significantly more than that from vapour phase.

Understanding the role played by solvent and supersaturation on growth morphology has attracted considerable interest during past two decades. These investigations essentially provide understanding of the crystal growth mechanism so that one can simulate the real scenario in crystallization processes and predict the growth shape. Nevertheless, the present theoretical and computational understanding of the mechanism through which solvent interacts with the surface is still not well understood.[13] It is also not clear that whether solvent inhibits[9-12] or promotes[4-7] the growth rate. In this direction, important contribution was made by Nielsen *et al*.[23], who have studied the effect of solvent to calculate rate of displacement by considering attachment and detachment frequencies of solvated GUs. Physically, these frequencies are associated with the type of solvated GUs and the structure of the growing face including the kink density on the crystal surface. Woensdregt[24] explained the effect of solvent on the growth rate in terms of impurity adsorption on the crystalline interface. Boek *et al*.[25] shows that the importance of the solute dynamics at the solvent-surface in order to define the growth units. The results of the MD simulation by Liu *et al*.[21] clearly shows that the analysis of the interfacial structure is crucial to investigate the effect of solvent on growth rate of urea crystal and formulated what is known as the interfacial structure analysis and predicted the growth shape of urea crystals in aqueous solutions. The concept of effective growth unit to predict the growth shape was first put forward by Liu *et al*.[21] They have carried out molecular dynamic simulations to produce the genuine interfacial structure in different crystallographic orientations. Gnanasambandam and Rajagopalan[26] extended the idea of Liu *et al*.[21], what is known as extended interfacial structure analysis, to predict the shape of α-glycine crystals from aqueous solutions by fully accounting the effects of solvent. More recently, Salvalaglio *et al*.[27] investigated the effect of solvent and tailor-made additive on the growth of urea crystal using MD simulation and show that nucleation can follows either a single-step or a two-step mechanism depending on the solvent.[28] On the other hand, the computational approach developed by Doherty *et al*.[29-31] is based on detailed analysis of Burton-Cabrera-Frank spiral growth mechanism[32] augmented by additional terms to account for the adhesion surface energy of the solvent at the interface. They have successfully applied their approach to predict the supersaturation dependent shapes of many organic crystals grown from solution. However their approach failed to predict shape of crystal when solvent interaction to the crystal faces is mostly electrostatic in nature. Wireko *et al*.[33] and Anwar *et al*.[34] have employed molecular dynamics simulations to study the growth rate of polar faces of α-resorcinol crystal from aqueous solution and showed that adsorption of water molecules is stronger on the slower growing face thus their results support the inhibition model of crystal growth. Working on similar lines, Hod *et al*.[35] have simulated the growth shapes of DL-alanine crystals from a mixture of aqueous solutions, with organic solvents such as isopropyl alcohol and ethanol. Schmidt *et al*.[36] have employed surface docking method to investigate the influence of water on the habit of benzoic acid crystals. They showed that 3-site water model was favoured for predicting the growth shapes. Piana *et al*.[37] have utilized multi-scale modelling to study the effect of solvent, supersaturation and extended defects on growth shape of urea crystal from aqueous and methanol solutions. They have demonstrated that the accounting for the molecular kinetics is important to

correctly calculate the growth morphology of urea crystal. Tóth[38] has combined the genetic algorithm and kinetic Monte Carlo simulations to determine molecular rate constants to obtain growth of urea in aqueous and methanol solutions. These studies clearly show that it is possible to investigate the effect of solvent and supersaturation on the crystal growth shapes. However use of their approach within the affordable computational time to calculate reliable rates for the crystallization is difficult.[39] Recently we have studied solvent-induced habit modification of different molecular crystals.[40] A comprehensive account of molecular modelling techniques based on computer simulations and computational chemistry has been made by Myerson[41] and Docherty and Meenan.[42]

In the present paper, a growth model, based on the inhibition mechanism in which interaction of solvent molecules to the crystal surface impede the growth rate, has employed to simulate the crystal shape by taking into the account of solvent and other external growth parameters. For this purpose, the idea of effective growth unit proposed by Liu *et al*.[21] has been extended in order to calculate molecular attachment energies on the crystal surfaces. The calculations of growth rates require knowledge of solute-surface and solvent-surface energies which are obtained from the analysis of interfacial structure.

3 Methodology

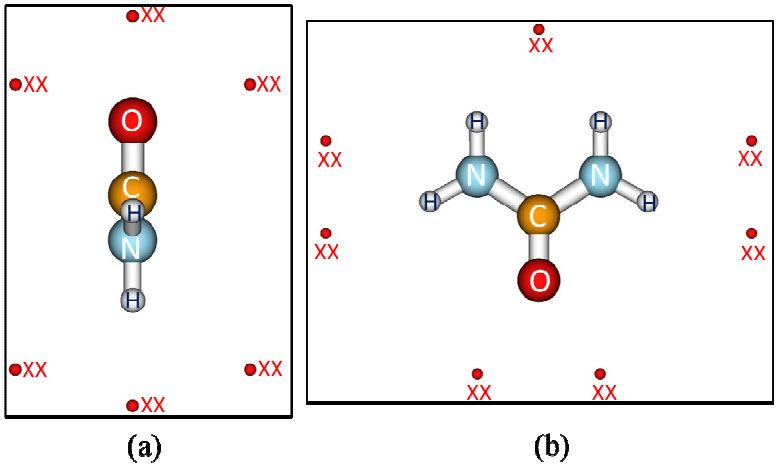

Figure 1. Two differently oriented assembly of urea molecules in (110) face of urea crystal. The vacancies (small red) are labelled by XX.

It is interesting to note that in reality, depending upon the degree of supersaturation, monomer, dimer or cluster of solute molecule is absorbed during the growth. Keeping this in mind, a methodology is presented for accurate calculation of molecular attachment energies (MAE) of the growth units taking particular care of its molecular orientation. The growth unit diffuses towards the interfacial region through mother nutrient and converted into a transient growth unit in the interfacial region. The growth unit also re-orients itself according to the atomic structure of the crystal face before it gets absorbed. The growth unit comprises of a solute molecule and neighbouring solvent molecules. Figure 1 depicts typical assemblies of urea molecules of different orientation at (110) face of the urea crystal. The vacancies are depicted by XX in Figure 1 which are points in space with an associated basis set, but lacking nuclear charge so allowing better description of the electron density in the vacancy. In case unit cell consists of

multiple molecules, MAE of each molecule may differ and depend on the relative orientation of molecules at the face. The MAE of the molecule is the energy released when molecule is adsorbed at the crystal surface, which is define as $E_{s-s}^{(hkl)} = (E_{cohesive} - E_{molecule}^{(hkl)})/2$, where $E_{cohesive}$ is cohesive energy of the crystal and $E_{molecule}^{(hkl)}$ is the difference between the energies of the isolated molecules on the slab and in the vapour/solution phase conformation. $E_{molecule}^{(hkl)}$ is calculated by converting neighbouring atoms into vacancies.[22] The growth rate of the face is determined by the adsorption of molecules having lowest MAE. Molecules having higher MAE have higher growth rate and lower morphological importance. This is in contrast to the HP model,[17] where it is assumed that each molecule in a face's unit cell has equal MAE in spite of different neighbouring vacancies. The MAE of molecules in different slabs have determined rather than the MAE of slabs as suggested by HP model.

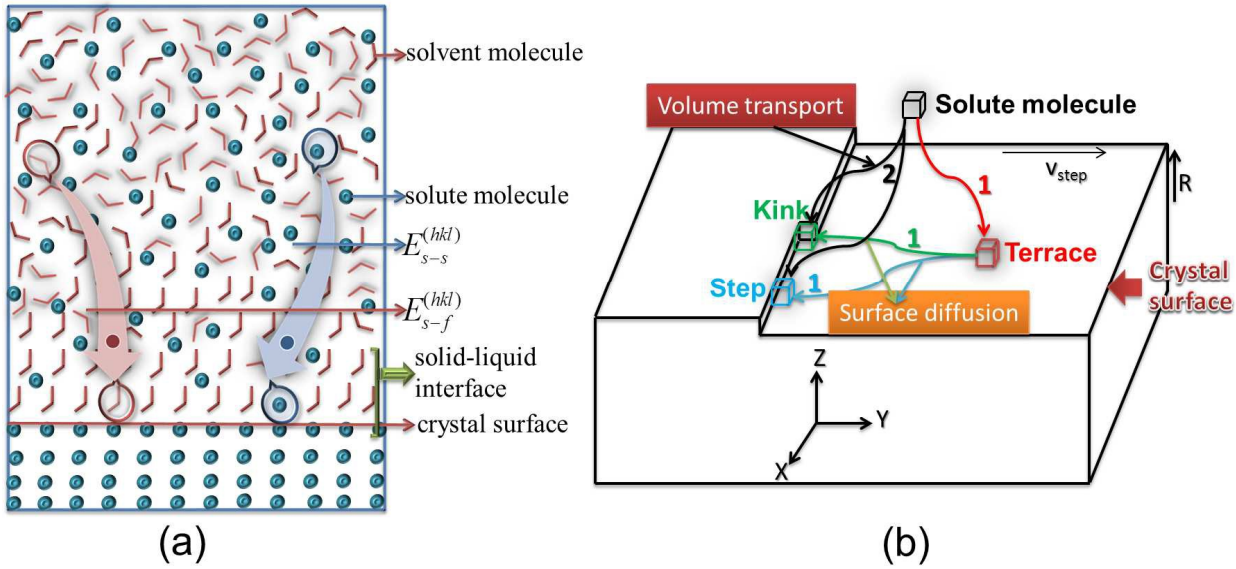

Figure 2. Schematic diagram showing (a) how crystal growth occurs from the solution method; Solvent molecules experience periodic potential near the crystal surface and causes formation of liquid layer. The incorporation of solute molecules in the crystal surface experiences a barrier which causes delay in the crystal growth. $E_{s-f}^{(hkl)}$ is the energy required to remove a bound solvent molecule attached to the surface (b) different sites for the attachment of solute molecule at a flat interface from vapour and solution phases.

The following methodology has been carried out to calculate MAE of the molecules in different faces of a crystal. A slab having two ideal semi-crystals has been created, each limited by an ideal surface which is parallel to the given plane (*hkl*). The charge neutrality of the slab is maintained during the process of slab generation. The origin is moved in order to minimize the number of symmetry operators with finite translation components. This is required before cutting a slab from 3-D structure. The physical slab must possess minimum energy configuration and zero dipole moment perpendicular to its surface. Note that configurations with a dipole moment perpendicular to the surface are rejected since their surface energy is infinite. The stability of the slab depends on its orientation, number of atomic layers and accurate surface termination. The number of atomic layer in a slab is determined by its inter-planer spacing, d_{hkl}. While creating a slab for the given orientation (*hkl*), often more than one surface termination

is possible. To determine the correct surface termination of a given slab, above discussed criterion are used to fix the surface atom of a slab. In most cases these conditions are satisfied at the same configuration. Each semi-crystal preserves 2-D periodicity parallel to the selected face, but loses all symmetry elements, which involve displacements in a perpendicular direction. The crystal surface that is taken as the starting point is not simply a straight cut from a zero temperature crystal structure, but fractions of cut molecules are recombined to complete molecules and the resulting configuration is not favoured energetically. To obtain a stable configuration, the integrity of the cut molecules in the slab needs to be restored. For this purpose, structural information about the complete molecules in the slab like bond lengths, bond angles and dihedral angles are utilised to calculate required displacements of the fragmented atoms in 2D unit cell. The details of the methodology employed to construct slabs having different orientations to determine MAE of the solute molecule is descried elsewhere.[22]

Following, we present a crystal growth model to study the effect of solid-liquid interface and external growth parameters on rate of growth from solution growth technique. Figure 2a shows a schematic diagram of the growth model. The crystal face provides a periodic potential at the crystal surface causes the adsorption of liquid molecules. At the crystal surface, periodic arrangement of solute molecules deviates from ideal structure of the face because the adsorption of liquid molecules also provides a periodic potential to the surfaces. The solid-liquid interface comprises an ordered arrangement of solid and liquid molecules at the crystal surface. Diffusion of the solvated growth units and solvent molecules experience a hindrance due to the formation of double layer. The crystal growth, for instance, takes place by the adsorption of GUs to the growth sites (kinks of steps) on the crystal surfaces after diffusion of GUs across the double layer from the bulk solution. In the immediate proximity of the crystal surface, a rigid Helmholtz-Stern layer is developed which consists of strongly adsorbed solvent molecules to the surface and partially solvated GUs. The solvated GUs penetrate into this layer after partially losing their solvation sheath and are specifically adsorbed at the surface for their growth. The released solvent molecules start counter-diffusion through the layer after the integration of GUs into the surface. Thus the attachment of solute molecules requires removal of solvent molecules from the interfacial region. The energy needed to detach a bind solvent molecule to the crystal surface at the kink/step sites is defined as binding energy of the solvent molecule, $E_{s-f}^{(hkl)}$ (cf. Figure 2a). The growth rate is limited by the removal of strongest bind solvent molecule to the surface. Figure 2b schematically depicts different growth processes take place during crystallization from vapour and solution phases. The route depicted by "1" represents two step process for vapour growth in which GUs first adsorb at the crystal surface and diffuse towards step/kink sites for their incorporation. However, route "2" shows that GUs in the mother phase directly transported at the steps/kink sites from the solution. A GU adsorbed at surface terrace, a smooth ledge and a kink site, has one, two and three out of the six nearest neighbours, respectively. Therefore, a solute molecule arriving on the surface terrace, at the terrace ledge and at the kink simply loses one, two and three degrees of freedom, respectively.

To model the solid-liquid interface of urea crystal, following set of operations have been performed. First, the initial structure of urea-water has been obtained from the chemical binding energy data of the systems available in the literature.[43] The stable configurations of different interfacial structure have been obtained by keeping in mind the positional disorder characteristic of the solvent molecules adsorbed on the crystal surface. Several positions and orientations of the water molecules have been tested

before obtaining stable configurations. The configurations thus obtained are structurally optimized using CRYSTAL09.[44] It is interesting to note here that the optimized interfacial structures of urea and water are in broad agreement with the results obtained from molecular dynamics simulations by Boek *et al*.[25] Figure 3 (panel a, b, c and d) show the optimized urea-water interfacial structures of (a) (001), (b) (110), (c) (111) and (d) $(\bar{1}\bar{1}\bar{1})$ orientations of urea crystal. The orientation of urea molecules adsorbed at different growth sites are represented by M1 and M2. On the other hand, different oriented water molecules at the top of above mentioned surfaces are represented by m1, m2 and m3. Hydrated models of the urea surfaces are examined by positioning a monolayer of water molecules above the surfaces, and then allowing the urea surface and water to relax to their minimum energy configuration. The determination of interfacial structure is restricted up to adsorption of one monolayer of water molecules at different surfaces of urea crystal primarily because the ordering of the water molecules are strongest near the crystal surface and disappears towards the bulk liquid. Thus it is expected that strongly bonded water molecule should be closest to the surfaces and hence affect the growth of faces. As can be seen in Figure 3a that two out of four of the hydrogen is involved in hydrogen bonds linking the urea molecules within the layer. The other two hydrogen and are buried within the layer and emerges at the opposite side of the face. It is clear from the Figure 3b-d that one out of two of the hydroxyl hydrogen and oxygen is involved in hydrogen bonds. The remaining hydroxyl hydrogen and oxygen are suppressed within the layer and appears at the opposite side of the faces.

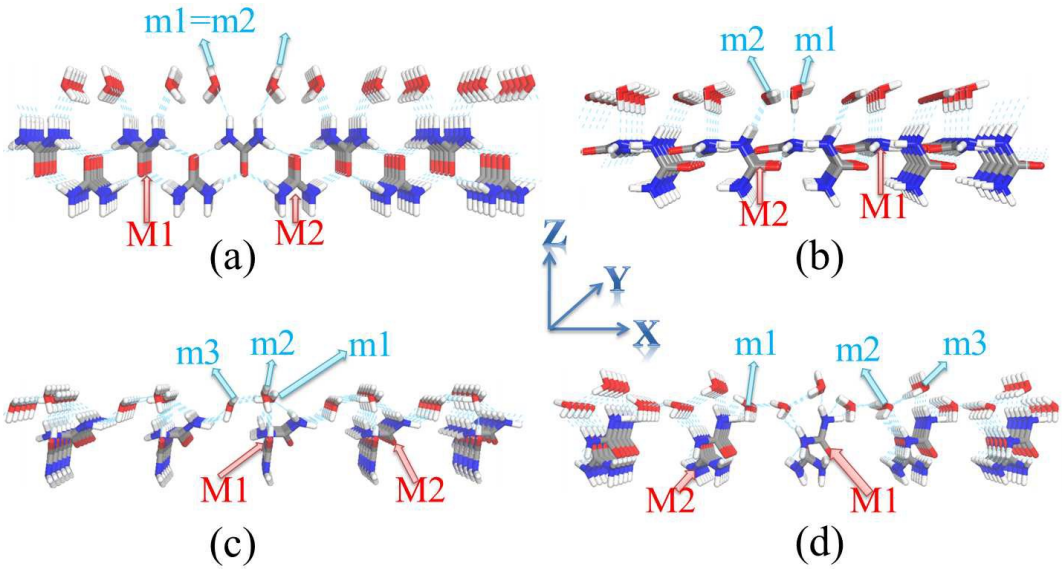

Figure 3. Optimized atomic structure of the crystalline urea-water interfaces of (a) (001), (b) (110), (c) (111), (d) $(\bar{1}\bar{1}\bar{1})$ surfaces. The strength of water molecules adsorption to (001), (111) and $(\bar{1}\bar{1}\bar{1})$ surfaces of urea crystal is one order weaker than the strength of binding of water molecules at (110) surface.

Based on the above discussion, interfacial structures of different crystal faces have determined and rigorous structural optimization has been carried out to determine the optimized interfacial structure. Periodic supercells of various sizes 1x1, 2x2, 3x3, 4x4 and 5x5 are constructed from the optimized interfacial structures and a water molecule is removed from the centre of the supercells to determine $E_{s-f}^{(hkl)}$. HF and DFT with hybrid exchange-correlation functional (B3LYP) (hereafter DFT-B3LYP) using all electrons Gaussian basis set has been employed to calculate $E_{s-s}^{(hkl)}$, $E_{s-f}^{(hkl)}$ and a counterpoise correction

method has been used to correct the basis set superposition error (BSSE).[45] It is well known that the all known exchange-correlation functional are unable to properly account for dispersive interactions,[46,47] but they are supposed to perform well when the interaction energy is dominated by electrostatics, as should be the case of hydrogen bonded (HB) molecular crystals. In this respect, urea crystal with their extended HB network is expected to be dominated by electrostatics. To address this shortcoming of the *ab initio* calculations, we have employed post self-consistent field (SCF) method[46,48] has employed to recover dispersion energy in urea crystal. BSSE plays an important role in binding of weakly interacting molecules. The binding energy of the water dimer obtained using HF approximation and employing small basis set is in good agreement with experiment.[46] With small basis sets the BSSE is large and gives an extra-binding that compensates for the missing dispersion energy but when large basis sets are employed, the reduction of the BSSE removes the spurious attractive interactions between the molecules, leading to an improper cancellation of the repulsive interactions. With this in mind, relatively smaller basis set (6-31G(d,p)) has been employed to calculate dispersion energy from HF and DFT method in order to obtain $E_{cohesive}$ and $E_{molecule}^{(hkl)}$ of urea crystal. To calculate BSSE, all atoms within the 3rd nearest neighbours of at least one atom in the molecule are converted into vacancies. The BSSE correction is restricted only up to 3rd neighbours since the lattice energies thus obtained are in good agreement with experimental enthalpy of sublimation. The calculated cohesive energies of urea crystal from HF and DFT methods are -21.3 kcal mol^{-1} and -27.0 kcal mol^{-1}, respectively. The cohesive energy obtained using HF method is in agreement with the experimental sublimation enthalpy (-21.0 kcal mol^{-1}).[49] The lattice cell parameters are determined to further test the validity of the computational method adopted in the present paper. The optimized lattice cell parameters (a=5.565 Å and c= 4.671 Å) are in good agreement with the experimental result (a= 5.576 Å, c= 4.684 Å).[50]

4 Computational Details

CRYSTAL09 program[44] has been employed to calculate relaxed interfacial structures and energetics of different crystal faces. The 6-31G(d,p) molecular all-electron basis set has been employed in the present calculation. The level of accuracy in evaluating the Coulomb and exchange series is controlled by five thresholds, which are taken to be 10^{-10}, 10^{-10}, 10^{-10}, 10^{-10}, 10^{-20}. The DFT exchange-correlation contributions are evaluated by numerical integration over the cell volume. The SCF ends when the root mean square (RMS) of the change in eigenvalues from two subsequent cycles is less than 10^{-10} hartree or the change in the absolute value of the total energy is less than 10^{-9} hartree. The shrinking factors along the reciprocal lattice vectors are set to 2, 2, 2, corresponding to 8 reciprocal space points of the irreducible Brillouin zone at which the Hamiltonian matrix is diagonalized. The experimental crystal structure of urea crystal[50] is used as initial guess to calculate the relaxed structure of 3-D bulk crystal and 2-D slabs of various orientations. Both lattice and atomic coordinates have been fully relaxed by means of numerical and analytical energy gradients, respectively. The geometry optimization is performed by means of a quasi-Newton algorithm in which the quadratic step is combined with a parabolic fit. Geometry convergence is tested on the RMS and the absolute value of the largest component of the gradients and estimated displacements. The threshold for the maximum force, the RMS force, the maximum atomic displacement, and the RMS atomic displacement on all atoms have been set to 0.00045, 0.00030, 0.00180 and 0.00120 au, respectively. The optimization is successfully completed when all four conditions are simultaneously satisfied. The symmetry is maintained during the surface relaxation process.

5 Results and Discussion

In order to study the solvent-induced crystallization at molecular-scale, we need to connect kinetic and thermo-dynamical aspect of the adsorption of solute and solvent molecules at the crystal surface. With this in mind, we derived a growth rate expression to calculate rate of growth of crystal faces by considering various external and internal growth factors affecting rate of growth. At low supersaturation, the growth of crystal facets is usually governed by the spiral growth mechanism.[32,51,52] With a monomolecular lateral step velocity of $\mathbf{v}_{step}^{kink(hkl)}$, step spacing λ_0, and a step height $h^{(hkl)}$, the growth rate normal to surface is given by, $R_{red}^{(hkl)} = \mathbf{v}_{step}^{kink(hkl)} h^{(hkl)} / \lambda_0$.[32] The step spacing is given by, $\lambda_0 \cong 19 \frac{\phi_{step}^{(hkl)} V_m}{kT \ln(1+\sigma)}$, where $\phi_{step}^{(hkl)}$ is the interfacial free energy, V_m the volume of the molecule, σ is the degree of supersaturation.[51,52] It follows that the growth rate of facet is given by, $R_{red}^{(hkl)} \propto \left(N_{step}^{(hkl)} - N_{step}^{eq(hkl)} \right) a\Gamma_k h^{(hkl)} \ln(1+\sigma)$, where $a\Gamma_k$ is the kink density.[53] The lateral step velocity is determined by the net flux of molecules entering ($N_{step}^{(hkl)}$) and leaving ($N_{step}^{eq(hkl)}$) at kink sites in the step.[54] At equilibrium, the flux of impinging molecules is equal to the flux of molecules leaving the surface. The step height is usually to be mono-molecular height[55] and usually corresponds to interplanner distance, d_{hkl}.[21(b)] The incorporation of the solute molecules are hindered by the occurrence of ordered liquid layer formed near the crystal surface usually known as interfacial-layer. It acts as a barrier through which solute molecules have to penetrate before they can be incorporated into the surface.[56] Due to the formation of interfacial-layer, not all flux of bulk solute molecules are seen by crystal surface but rather a fraction of them. It depends on many parameters like, equilibrium and supersaturated concentration of solute molecules, $E_{s-s}^{(hkl)}$, $E_{s-f}^{(hkl)}$ and diffusion layer thickness and is given by $N_{step}^{(hkl)} \propto c^3 E_{s-s}^{(hkl)} / \left(c^2 c_{eq} E_{s-s}^{(hkl)} + E_{s-f}^{(hkl)} \right)$. Here, it assumed that the solute concentration is uniform throughout the solution which is realized under intense force convection. However, a general expression of solute concentration limited by bulk diffusion at kink site is given by Chernov bulk diffusion model.[57] With c and c_{eq} are the mole fraction of solute per solvent molecule in supersaturated and saturated solution, respectively, the effective reduced growth rate, $R_{red}^{(hkl)}$ is given by,

$$R_{red}^{(hkl)} \propto \frac{2Td_{hkl} \ln(1+\sigma)}{\phi_{step}^{(hkl)}} \frac{\left[\frac{c_{eq}^3 (1+\sigma)^3 E_{s\text{-}s}^{(hkl)}}{c_{eq}^3 (1+\sigma)^2 E_{s\text{-}s}^{(hkl)} + E_{s\text{-}f}^{(hkl)}} - \frac{c_{eq}^3 E_{s\text{-}s}^{(hkl)}}{c_{eq}^3 E_{s\text{-}s}^{(hkl)} + E_{s\text{-}f}^{(hkl)}} \right]}{\left(2 + \exp\left(\frac{\phi_{step}^{(hkl)}}{RT} \right) \left(\frac{\cosh\left(\frac{\phi_{step}^{(hkl)}}{RT} - 0.5 \ln(1+\sigma) \right)}{\cosh\left(\frac{\phi_{step}^{(hkl)}}{RT} + 0.5 \ln(1+\sigma) \right)} \right)^{\frac{1}{2}} \right)} \quad (1)$$

With saturated mole fraction of solute concentration c_{eq}, the supersaturation, σ for practical purposes can be approximated as,

$$\sigma = \left(c - c_{eq} \right) / c_{eq} \quad (2)$$

where R, T, n_{hkl}, $E_{cohesive}$, ΔH^{diss}, $E_{s-s}^{(hkl)}$ and $E_{s\text{-}f}^{(hkl)}$ are the gas constant, temperature, coordination number, cohesive energy, bulk enthalpy of dissolution, adsorption energy of solute and solvent molecules at the crystal surface, respectively. c_{eq} is usually determined from the solubility data at a given temperature. The step energy per mole of molecules, $\phi_{step}^{(hkl)}$ is the energy required to create a one dimensional step of height similar to that of size of one molecule and it can be related to the local dissolution enthalpy, $\Delta H_{(hkl)}^{diss}$, at the surface.[21] In the rotating spiral, step energy depends on the molecular orientation of the solute molecules. It is given by,[21(b)]

$$\phi_{step}^{(hkl)} \approx \left(\frac{E_{(hkl)}^{slice}}{E_{cohevive}}\right)\left(\frac{\Delta H_{(hkl)}^{diss}}{\Delta H^{diss}}\right)\frac{\Delta H^{diss}}{n_{hkl}} \tag{3}$$

where the slab energy, $E_{(hkl)}^{slice}$ can be expressed as,[17]

$$E_{(hkl)}^{slice} = \left(E_{cohesive} - E_{s-s}^{(hkl)}\right) \tag{4}$$

As mentioned earlier that we are no longer using hypothesis of the HP model in which slab energy is well defined quantity which represents aggregate lateral binding of the solute molecule in the plane of 2-D slabs. However, in the present approach, we still can define an energy analogues to the slab energy. The lateral binding of solute molecules depends on the adsorption energy of solute molecules in the growing steps. Moreover, the effective concentrations of solute and solvent molecules near the crystal surface are different from the corresponding value in the bulk phase due to the development of the diffusion boundary layer and solid-liquid interface near crystal surfaces.

Adsorption of solute and solvent molecules on the flat crystal surfaces are controlled by three parameters, namely, thermodynamic, kinetic factors and the solubility. It is usually assumed that above mentioned parameters determined the step energy. In our previous calculations,[40] role of solid-solvent interaction, solute and solvent concentrations were neglected to calculate step energy. It is clear from Eq. (3) that the step energy depends on the local dissolution enthalpy at the crystal surface, which, in turn, depends on the concentration of effective growth units in solutions.[21] The adsorbed solvent molecules at the kink sites of the growing step cost an additional energy barrier which leads to increase in step energy.[58] Consequently the incorporation of solute molecules to the growing steps experiences difficulty. Moreover, increasing the supersaturation decreases the step energy until it vanishes.[27] Also, an increase in solubility leads to a decrease in strep energy which eventually increase the rate of growth. Keeping above discussion in mind, the average step energy has the form,

$$\phi_{step}^{(hkl)} \approx \left(\frac{E_{cohevive} - cE_{s-s}^{(hkl)} + \frac{1}{c}E_{s-f}^{(hkl)}}{E_{cohevive}}\right)\frac{\Delta H^{diss}}{n_{hkl}} \tag{5}$$

We now determine the effective concentration of solute molecules and local dissolution enthalpies at the crystal surface. The unit cell of urea crystal comprises two molecules and, thus, their relative orientation depends on slab orientation (*hkl*). The ratio of step energies of M1 and M2 oriented solute molecules can be related to their effective solute concentration. It can be expressed as,[21b]

$$\frac{\phi_{step(M1)}^{(hkl)}}{\phi_{step(M2)}^{(hkl)}}=\frac{\left(E_{cohevive}-cE_{s-s(M1)}^{(hkl)}+\frac{1}{c}E_{s-f}^{(hkl)}\right)}{\left(E_{cohevive}-cE_{s-s(M2)}^{(hkl)}+\frac{1}{c}E_{s-f}^{(hkl)}\right)}\cong\frac{\ln X_{M1}^{eff(hkl)}}{\ln X_{M2}^{eff(hkl)}}\equiv\frac{\ln\left(\frac{c_{M1}^{eff(hkl)}}{1+c_{M1}^{eff(hkl)}}\right)}{\ln\left(\frac{c_{M2}^{eff(hkl)}}{1+c_{M2}^{eff(hkl)}}\right)} \quad (6)$$

where X and c represent the bulk concentration of solute molecules in two different conventions. The former represents the mole fraction of solute per mole of solution whilst later denotes the mole fraction of solute per mole of solvent. The effective concentration of solute molecules having either M1 or M2 orientation in former and later convention is represented by $X_{M1}^{eff(hkl)}$, $X_{M2}^{eff(hkl)}$ and $c_{M1}^{eff(hkl)}$, $c_{M2}^{eff(hkl)}$, respectively. The solute concentration in solution can be written as,

$$c=c_{M1}^{eff(hkl)}+c_{M2}^{eff(hkl)} \quad (7)$$

Combining Eq.(6) and (7), we get,

$$\frac{c_{M1}^{eff(hkl)}}{1+c_{M1}^{eff(hkl)}}=\left(\frac{c-c_{M1}^{eff(hkl)}}{1+c-c_{M1}^{eff(hkl)}}\right)^{\left(E_{cohevive}-cE_{s-s(M_1)}^{(hkl)}+\frac{1}{c}E_{s-f}^{(hkl)}\right)/\left(E_{cohevive}-cE_{s-s(M_2)}^{(hkl)}+\frac{1}{c}E_{s-f}^{(hkl)}\right)} \quad (8)$$

From the van't Hoff relation,[59] we easily get expression for local dissolution enthalpy of M1 oriented molecule as,

$$\Delta H_{(hkl)M1}^{diss}\cong\left(\frac{\ln\left(\frac{c_{M1}^{eff(hkl)}}{1+c_{M1}^{eff(hkl)}}\right)}{\ln\left(\frac{c}{1+c}\right)}\right)\Delta H^{diss} \quad (9)$$

We can determine the effective concentration and local dissolution enthalpy by solving Eq. (8) and (9) iteratively. It is well known that the solubility of the crystal is greatly affected by the interaction energies of solvent-solvent, solute-solute and solute-solvent in bulk solution. Our approach considered the effect of solubility on rate of growth, thus, taking the aggregate effect of various interactions occur in the bulk phase. The detailed proposition to derive the above growth rate expression is reported elsewhere.[40] Continuing on the similar line of reasoning, we can easily extend the above expression for growth from impure solution containing tailor-made additives/impurities.[60]

Having established the growth rate expression, we now turn to calculate various habit controlling energies of solute and solvent molecules at different faces of the urea crystal. Figure 4a illustrates the crystal structure of urea crystal with noncentrosymmetric $P\bar{4}2_1m$ space group, with two molecules in the unit cell. Urea exhibits rich crystallization behaviour in spite of its simple molecular structure. The vapour and solution growth morphologies of urea crystals[21,22,30,37,39,61-65] have been extensively well studied. Docherty *et al.*[61] and Boek *et al.*[62] have predicted growth morphology of the urea crystal using HP model and considered only experimentally observed faces. On the other hand, George *et al.*[63] considered the others faces for calculating growth shapes, but they predicted the appearance of (101) and (200) faces and underestimated the morphological importance of (111) face. A methodology adopted by Bisker-Leib *et al.*[30] takes in to account of the anisotropy present in different slabs of the urea crystal. However, there have only considered experimentally observed faces and neglected the effect of surface relaxation on growth morphology of the urea crystal. The classical molecular dynamics and Monte Carlo simulations

have been employed to predict the solvent-induced growth morphology of the urea crystal by several research groups.[21,27,37] It has been established that the growth mechanism of different faces are different.[37] Their investigation essentially provides a framework to access the impact of solvent and additive on crystallization process.

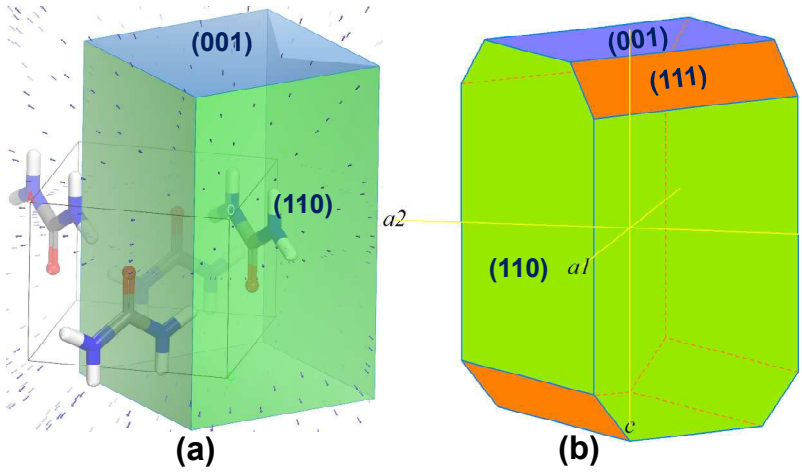

Figure 4. (a) Crystal structure and (b) experimentally observed growth morphology from vapour.[61]

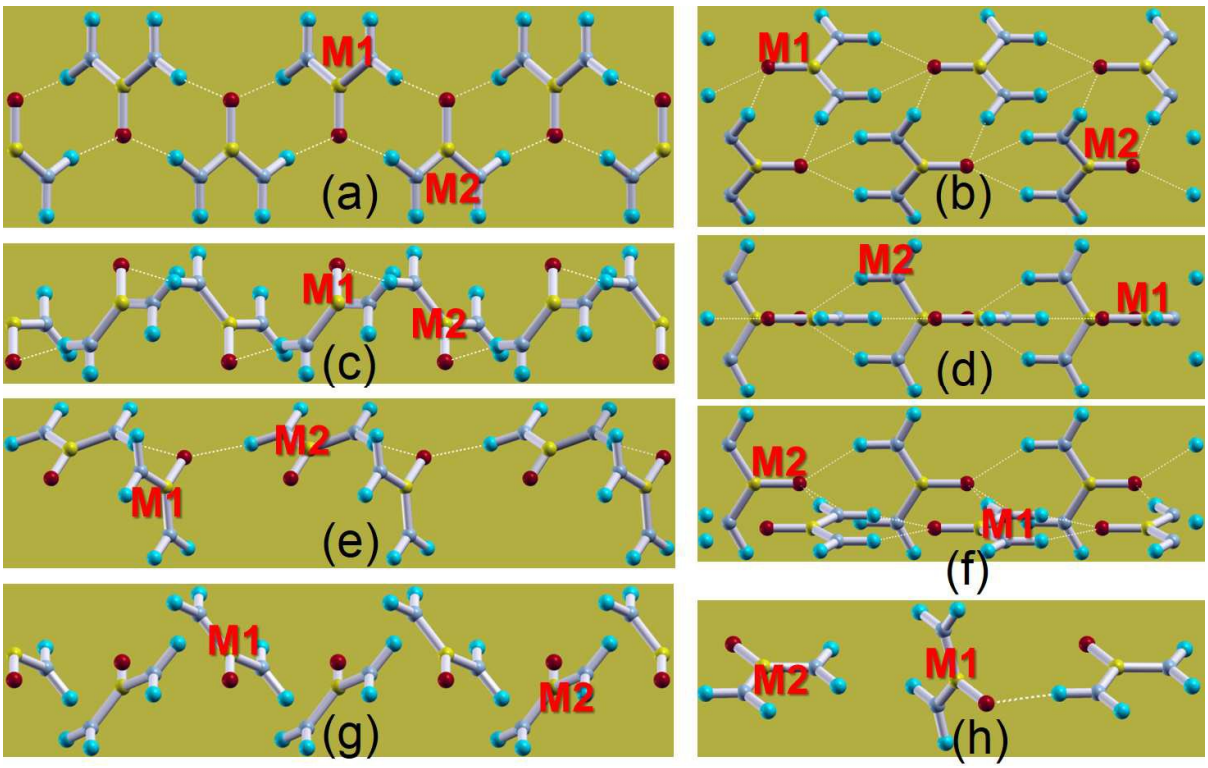

Figure 5. Relaxed slabs structure of urea crystal of faces (a) (100), (b) (110), (c) (101), (d) (001), (e) (111), (f) (210), (g) (201) and (h) (211). The molecular orientation of the urea molecules at different growth sites are represented by M1 and M2.

We first discuss the prediction of vapour growth morphology of the urea crystal. The predicted growth morphology of urea crystal using the HP model and semi-empirical force-field method is shown in

Figure 4a. No consideration of orientation of urea molecules in different faces has been made to compute corresponding slab energy and, hence the growth shape. A comparison with a shape drawn from a scanning electron micrograph of urea crystallized from the vapour phase,[61] as shown in Figure 4b, clearly reveals that the shape obtained using the HP model does not correspond to experimentally obtained morphology of the urea crystal. One can see the absence of (111) face from the predicted shape (cf. Figure 4a). The above discrepancy between the calculated and experimental growth shape as shown in Figure 4, can easily be resolved by taking care of the molecular orientation and surface relaxation while calculating MAE of differently oriented urea molecules in different faces. We recently investigated the effect of molecular orientation and surface relaxation of the habit faces to predict the growth morphology of molecular crystals.[22] Figure 5 (panel a-h) shows the optimized solid-vapour interfaces of (001), (10), (101), (110), (111), (210), (201), and (211) faces of urea crystal, respectively. The orientation of urea molecules adsorbed at different growth sites of above mentioned faces is represented by M1 and M2. The adsorption of M2 oriented molecule rate-limit the growth of (110) and (210) faces as MAE of M1 molecule is lower than that of the M2 molecule.[22] On the other hand, growth of (111) and (211) faces are rate-determined by the adsorption of M1 oriented molecule. The microscopic image of the growth morphology of the urea crystal can be obtained from the MAE of the rate-limiting molecules in different faces and using the prescription of HP model. Accordingly the growth rate of a face is proportional to the MAE of the rate limiting molecule on the crystal faces.[19] The predicted growth morphology obtained using the HF method correctly reproduce all the experimentally observed faces in the urea crystal and excellent agreement with the experimental results[61] has been established.[22a]

Table 1. Molecular attachment energy (kcal mol^{-1}) of urea molecules in M1 and M2 orientations at (111) and ($\bar{1}\bar{1}\bar{1}$) faces using HF method.

Face	MAE (kcal mol^{-1}) of urea molecule in orientation					
	without relaxation/reconstruction			with relaxation/reconstruction		
	M1	M2	M2 in presence of M1	M1	M2	M2 in presence of M1
($\bar{1}\bar{1}\bar{1}$)	-3.22	-1.10	-5.83	-5.32	-3.04	-7.94
(111)	-2.91	-1.34	-4.97	-4.39	-2.44	-6.93

We now examine the uneven growth of (111) and its Freidel opposite ($\bar{1}\bar{1}\bar{1}$) faces of the urea crystal. For these crystals, the growth rates of the faces delineating the polar axis are generally expected to be equal. Using the slab model, we show that the MAE at these faces of the urea crystal are equal to each other and polar morphology of urea crystal from vapour phase cannot be predicted using the slab model.[22] Owning different surface chemistry at these faces, as one would expect that it will eventually lead to the difference in polarization along the polar axis. As a result, the adsorption energies of solvent and solute and, hence, solvent-induced step energy at these faces are different which eventually leads to uneven rate of growth at these faces. Several models[66,67] have been proposed to address the uneven growth of (011)

and $(0\bar{1}\bar{1})$ faces of α-resorcinol crystal from the vapour phase. Recently, we employed molecular-scale model based on the surface docking approach to determine MAE of differently oriented GUs at the opposite and hemihedral faces of different acentric materials to examine the phenomena of uneven growth and dissolution and established that the phenomena of unidirectional growth and dissolution along the polar axis of α-resorcinol and urea crystals are fundamental properties to the acentric crystals.[68] Our approach has based on the fact that polarization along the polar axis is different and hence MAE of molecules on these faces is different. The detail of the calculations of MAE of M1 and M2 oriented molecules at (111) and $(\bar{1}\bar{1}\bar{1})$ faces of urea crystal are discussed in Ref. 68. The results for relaxed MAE of different orientations of molecules at these faces of the urea crystal using the HF method are compiled in Table 1. The rate-limiting MAE can be determined from the relation,[68]

$$\text{Rate-limit MAE} = max\left\{min\left(E_{M1}^{MAE},\ E_{M2}^{MAE}\right),\ E_{M2/M1}^{MAE}\right\} \qquad (10)$$

where E_{M1}^{MAE}, E_{M2}^{MAE} and $E_{M2/M1}^{MAE}$ are the MAE of solute molecules in orientation M1, M2 and M2 in the presence of M1 molecules, respectively. By using Eq.(10) and the results for MAE complied in Table 1, the polar morphology of urea crystal from vapour phase has been predicted, which is experimentally verified.[61] It is evident from Table 1 that the adsorption of M1 oriented molecule rate-limit the growth of (111) and $(\bar{1}\bar{1}\bar{1})$ faces for which the value of relaxed MAE are -4.39 and -5.32 kcal mol^{-1}, respectively.

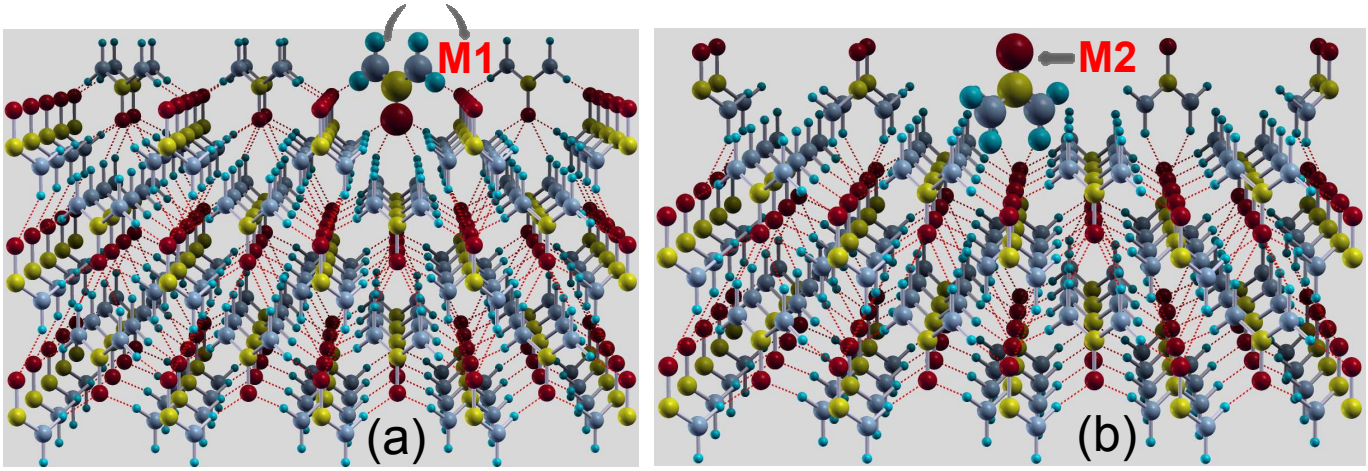

Figure 6. Schematic diagram showing the adsorption of GU of orientation (a) M1 and (b) M2 in the growing steps at (001) face of urea crystal from solution.

We next focus our attention on the investigation of aqueous growth of the urea crystal. To this end, (001), (110), (111) and $(\bar{1}\bar{1}\bar{1})$ faces are considered to determine $E_{s-s}^{(hkl)}$ and $E_{s-f}^{(hkl)}$. It is clear from Figure 2b that the solute molecules directly integrated at the growing steps/kink sites from the solvent-induced crystallization. Keeping this in mind, the study of solvent-induced crystallization requires accurate determination of the adsorption energy of solute molecules in the presence of the growing steps at different crystal faces. The adsorption energies of the urea molecule having M1 and M2 orientations (cf. Figure 1) in different step configuration along *a*- and *b*-latttice vectors of the 2-D lattice of corresponding faces are calculated by constructing 3x3 periodic supercell upon which M1 and M2 oriented urea

molecules are docked at their crystallographic position. The schematic illustration showing the adsorption of urea molecule of (a) M1 and (b) M2 orientation in the growing steps at (001) face of urea crystal is shown in Figure 6 (panel a and b). The structure of the adsorbed molecule in M1 and M2 orientations in the presence of M1 and M2 oriented molecules and *vice versa* in various step configurations at the above mentioned faces have also been optimized in order to calculate relaxed adsorption energies.

Table 2. Relaxed adsorption energy of M1 and M2 oriented urea molecules, $E_{s-s}^{(hkl)}$ (kcal mol^{-1}) at kink sites of the steps along a- and b-lattice vectors of different faces of the urea crystal at HF level of theory.

Face	Step direction	Adsorption energy, $E_{(hkl)}^{solute/surf}$ (kcal mol^{-1}) of urea molecule in orientation			
		M1 in presence of M1 (M1/M1)	M2 in presence of M2 (M2/M2)	M1 in presence of M2 (M1/M2)	M2 in presence of M1 (M2/M1)
(001)	*a*/*b*	-10.95	-4.14		
(110)	*a*	-6.91	-6.38		
	b			-6.77	-6.40
(111)	*a*/*b*			-5.85	-6.44
$(\bar{1}\bar{1}\bar{1})$	*a*/*b*			-7.16	-8.38

The results of relaxed adsorption energies of urea molecules in different steps configurations obtained at the HF level of theory are reported in Table 2. The optimized step configurations along 2-D lattice vectors are presented elsewhere.[60] It is evident from Table 2 that the adsorption energy along *a*- and *b*-lattice vectors of the 2-D slabs on (001), (111) and $(\bar{1}\bar{1}\bar{1})$ faces are equal to each other and, hence, step energies and rate of growth along either of the lattice vectors are same. In contrast to this, adsorption energy along the *a*- and *b*-lattice vectors at (110) face are different to each other. It can be seen from the results presented in Table 2 that the M2 oriented molecules nucleates on top of (001) face terminated by M1 molecules and *vice versa* for which the value of $E_{s-s}^{(hkl)}$ are -4.14 kcal mol^{-1} and -10.95 kcal mol^{-1}, respectively. The advancing spiral steps at (001) face is rate-limited by the adsorption of M2 oriented molecules as the adsorption energy of M2 molecule is lower than that of M1 molecule. On the other hand, adsorption of M2 molecule in the presence of M1 (M2/M1) along *b*-lattice vector rate-limit the crystallization of (110) face for which the value of $E_{s-s}^{(hkl)}$ is -6.40 kcal mol^{-1}. The adsorption energy of M1 oriented molecule in the presence of M2 molecule (M1/M2) along *a*- and *b*-vectors of the 2-D lattice at (111) face rate-limit the growth of (111) and $(\bar{1}\bar{1}\bar{1})$ faces. The relaxed adsorption energy of the rate-limiting molecules (M1/M2) at (111) and $(\bar{1}\bar{1}\bar{1})$ faces are -5.85 kcal mol^{-1} and -7.16 kcal mol^{-1}, respectively. It can be seen from the adsorption energy landscape of urea molecules that the successive

adsorption of M1 and M2 oriented molecules occurs at (110), (111) and $(\bar{1}\bar{1}\bar{1})$ faces for their growth. We have employed Eq.(5) along with the results presented in Table 2 to compute step energies at various supersaturation. The further investigation of step energy and growth rate of the urea crystal from pure and impure aqueous solutions containing biuret as additive at dispersion corrected DFT-B3LYP level of theory are reported elsewhere.[60]

Table 3. The binding energies of the strongly bind water molecules at the different surfaces of urea at HF level of theory. Periodic supercell model has been used and corrected values of $E_{s-f}^{(hkl)}$ are listed in parenthesis.

crystal face (*hkl*)	$E_{s-f}^{(hkl)}$ (kcal mol^{-1}) in supercell size of				
	1x1	2x2	3x3	4x4	5x5
(001)	-1.04	-1.65	-1.75	-1.77	-1.77 (-0.40)
(110)	-7.72	-8.14	-8.25	-8.34	-8.34 (-6.97)
(111)	-1.50	-1.80	-1.95	-2.03	-2.05(-0.73)
$(\bar{1}\bar{1}\bar{1})$	-1.45	-1.70	-1.78	-1.84	-1.87(-0.55)

Having discussed the results for the adsorption energy of solute molecules in different configurations of the growing steps, we now turn to calculate adsorption energy of water molecules at different faces of the urea crystal. In Figure 3 (panel a-d), we shows the optimized solvent-surface of the above mentioned faces. Table 3 lists the calculated $E_{s-f}^{(hkl)}$ and corrected values of $E_{s-f}^{(hkl)}$. The energy correction in $E_{s-f}^{(hkl)}$ is made for a single H-bond energy (-1.38 kcal mol^{-1}) of ice-like water molecule[69,70] and are shown in parenthesis in Table 3. It is clear from Table 3 that the binding energy of water at (110) face is significantly higher than that of (001), (111) and $(\bar{1}\bar{1}\bar{1})$ faces. As can be seen from Figure 3b and Table 3 that the water-urea configuration at (110) face corresponds to minimum energy configuration.[43] Åstrand *et al.*[43] show that the water-urea binding energy in minimum energy configuration of urea-water dimer possess -10.9 kcal/mol. The water molecule is engaged in two hydrogen bonds with urea at (110) face. However, only one hydrogen bond formed between water and urea molecule at the surfaces of (001), (111) and $(\bar{1}\bar{1}\bar{1})$ faces. Our results show that the hydrogen bond length of the strongly adsorbed water molecule at (110) face are lower than that of (001), (111) and $(\bar{1}\bar{1}\bar{1})$ faces. In Figure 7 (panel a and b), we show the calculated step energy, $\phi_{step}^{(hkl)}$ and local dissolution enthalpy, $\Delta H_{(hkl)}^{diss}$ of the adsorption of M1 and M2 oriented urea molecules in the rotating spiral at (a) (001) and (b) (110) face at different supersaturation. The bulk enthalpy of dissolution of urea crystal in aqueous solution is 4.02 kcal/mol.[71] As can be seen in Figure 7 that the step energy decreases with increasing supersaturation. The M1 oriented urea molecules at (001) face has higher step energy than that of M2 oriented molecules and, thus, growth rate of (001) face is rate-limited by the adsorption of M1 molecule. Moreover, M1 oriented molecule at

this face has lower effective concentration (not shown) and higher local dissolution enthalpy than that of M2 oriented molecule. On the other hand, it is evident from Figure 7b that the step energy and local dissolution enthalpy of urea molecule in M2 orientation at (110) face take higher value than that of M1 oriented molecule and the rate of growth of (110) face is rate-determined by the adsorption of M2 oriented molecules in the growing steps along *b*-lattice vector (cf. Table 2).

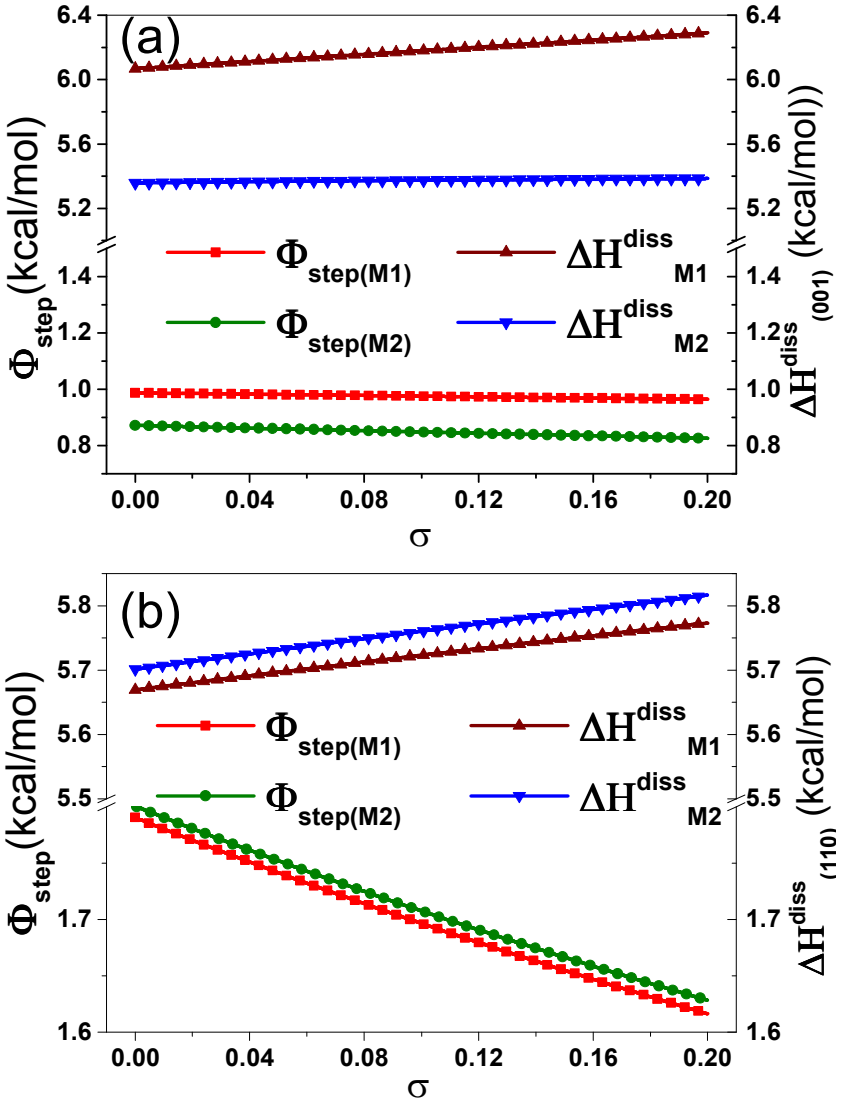

Figure 7. Step energy and local dissolution enthalpy of the adsorption of differently oriented urea molecule in (a) (001) and (b) (110) faces.

Along with the results presented in Tables 2 and 3, we employed eq. (1) to calculate growth rate of (001) and (110) faces versus σ at different saturation temperatures, which are sketched in Figure 8. As can be seen from Figure 8 that the spiral growth mechanism is viable mechanism for (001) and (110) in low σ regime while linear growth mechanism is applicable at higher σ, consistent with growth rate data by Davey *et al.*[64] It also reveals that growth rate of (110) face ($R_{red}^{(110)}$) is negligible at low σ since adsorption energy of the water molecule to this surface is stronger than that of (001) and (111) surfaces, which is in agreement with the experimental observation.[64] The strong interaction of water molecule to the

(110) surface is primarily responsible for the inclusion occurs at this surface rather than either (001) or (111) faces. It is evident from the Figure 8 that width of dead zone on (110) face decreases upon increasing the saturation temperature. At higher σ, $R_{red}^{(110)}$ increases rapidly due to the kinetic roughing, as shown by Piana *et al*.[37] The aspect ratio $\left(AS = R_{red}^{(001)} / R_{red}^{(110)}\right)$ as a function of σ at different saturation temperatures (T) is shown in the inset of Figure 8. It is interesting to note that at extremely higher σ, shape of the urea crystal changes from needle $\left(AS \cong 60\right)$ to block like $\left(AS \cong 1.55\right)$ habit. Our calculations show that the increase in σ result a decrease in aspect ratio. The increase in saturation temperature results an increase in growth rates but decrease in aspect ratio. At low supersaturation, Figure 9 (panel a, b and c) shows the simulated habits of the aqueous grown urea crystals at saturation temperature (a) 20 ^{o}C (b) 25 ^{o}C and (c) 40 ^{o}C. The predicted growth habit of the urea crystal from aqueous solution is in good agreement with the experimental result.[64] Finally, we show our predicted vapour growth shape in Figure 9d in order to compare with aqueous growth habit. The calculated aspect ratio of aqueous grown urea crystal (~60) is well matches with the experimental observation.[64] The growth of KDP crystal from aqueous solution also shows the similar behaviour.[72] The binding energy of water molecules to (101) facet is higher than (100) of KDP crystal[73] is similar to the case of urea crystal in which binding energy of water molecules to (110) facet is higher than (001).

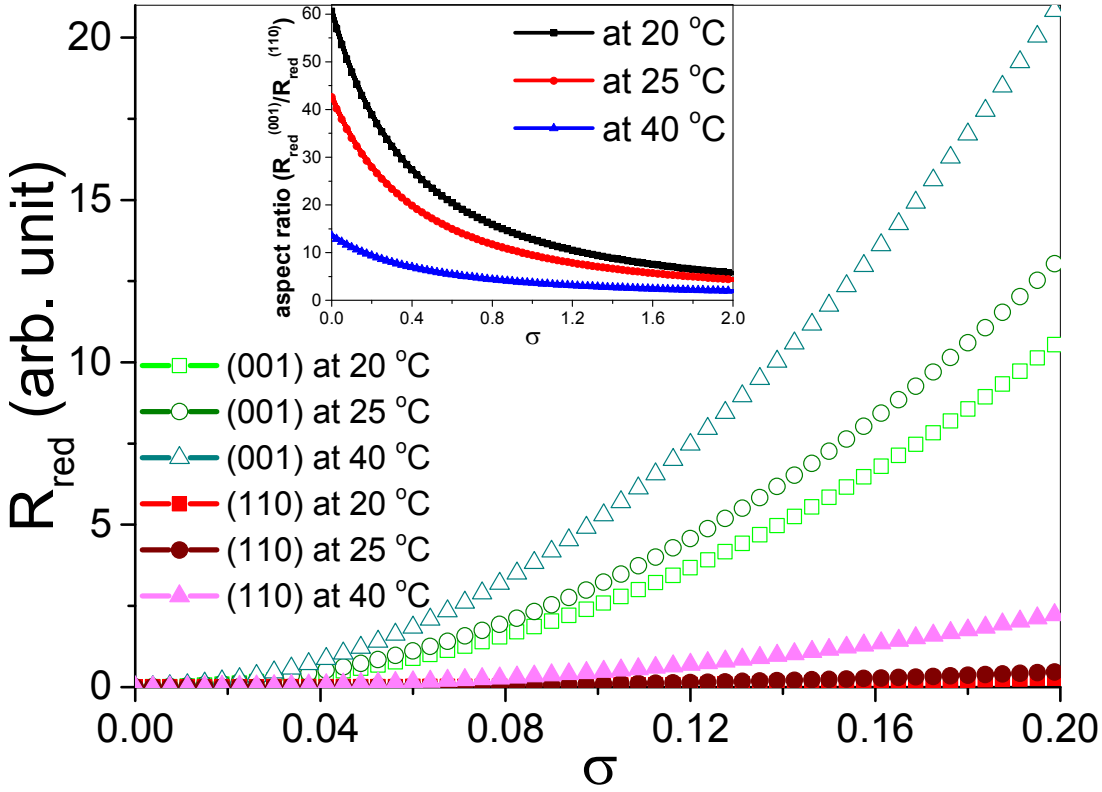

Figure 8. Reduced growth rates of (001) and (110) facets of urea crystal from aqueous solution as a function of σ at various saturation temperatures. The aspect ratios versus σ at different saturated temperatures were shown in inset. The shape of urea crystal becomes needle like at low σ and acquire block like shape at higher σ.

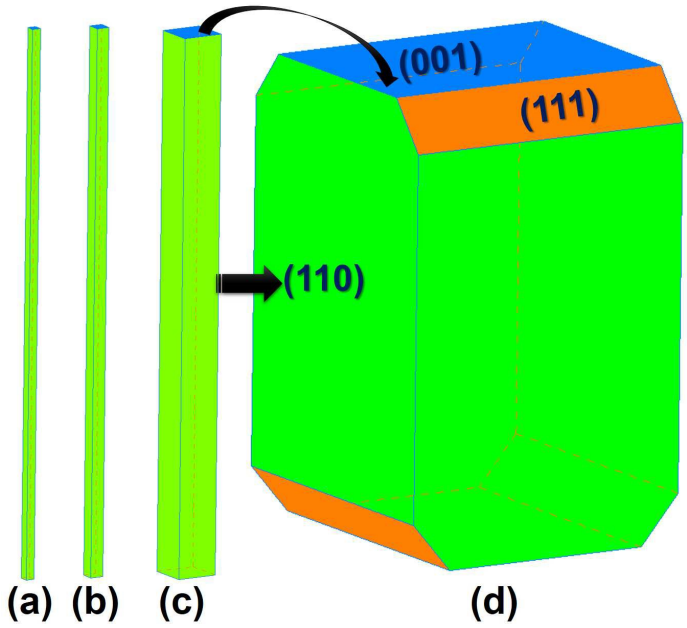

Figure 9. Predicted growth morphologies of urea crystal using HF method at lower supersaturation and at temperatures (a) 20 °C (b) 25 °C (c) 40 °C from aqueous solution and (d) vapour phase growth morphology from our results. The calculated aspect ratio is in agreement with experimental[64] *and simulated results by others.*[21b,37]

6 Summary and Conclusions

In summary, we have examined growth morphology of the crystalline urea from vapour and aqueous solution considering the effect of crystallographic parameters, solid-liquid interfacial structure and external growth parameters. The binding energies of solid-solid and solid-liquid are calculated within the framework of presented model using first-principles method. Our calculations for habit controlling energetics include the effect of molecular orientation of growth units and surface relaxation of different habit faces. Several step configurations along 2-D lattice vectors at different crystal surface has been examined before obtaining accurate adsorption energy of the solute molecule in the growing steps. In aqueous solution, calculations of step energy, effective concentration of solute molecule and local dissolution enthalpy at different degree of supersaturation of differently oriented solute molecules have carried out. The growth morphologies of the urea crystals grown from vapour and aqueous solution have investigated within the framework of discussed model. Our results show that the development of block and needle-like habits from vapour and aqueous solution, respectively which is in good agreement with the experimentally obtained morphologies of urea crystal. In aqueous solution, we find that the length to breath aspect ratio of the urea crystal decreases on increasing σ and T is consistent with experimental observations. Our results conclusively established the role of solid-liquid interfaces, orientation of solute molecules, supersaturation, temperature, and solubility on the growth morphology. Thus, it paves the way for the predictive design of crystal growth experiments. We believe our proposed method and presented results will lead to further theoretical as well as experimental studies in crystal growth.

Acknowledgment: The author is grateful for the support and motivation received from P. K. Gupta. Discussion with V. S. Tiwari and Arup Banerjee are gratefully acknowledged. The anonymous referees for this paper are also thanked for their helpful comments and suggestions that have helped us to improve the paper. All the calculations have been performed on Brahma, Nalanda, Kshitij-2, and 3 Linux clusters at our centre.

Reference:

1. B. Bhushan, J. N. Israelachvili and U. Landman, *Nature*, 1995, **374**, 607-616.
2. E. Johnson, *Science,* 2002, **296**, 477-478.
3. E. Vlieg, *Surf. Sci.,* 2002, **500**, 458-474.
4. J. R. Bourne, R. J. Davey, *J. Crystal Growth*, 1976, **36**, 278-287.
5. J. R. Bourne, R. J. Davey, *J. Crystal Growth*, 1976, **36**, 287-296.
6. P. Bennema, J. P.van Eerden, in *Morphology of Crystals*, Terra Scientific Publishing Co., Tokyo, 1977, pp 1-75.
7. (a) L. J. W. Shimon, M. Vaida, L Addadi, M. Lahav, L. Leiserowitz, *J. Am. Chem. Soc.*, 1990, **112**, 6215-6220. (b) M. Lahav and L. Leiserowitz, *Cryst. Growth Des*., 2006, **6**, 619–624.
8. P. Bennema, G. Gilmer, in *Crystal Growth: An Introduction*, ed. P. Hartman, North-Holland, Amsterdam, 1973, p 274.
9. I. Weissbuch, R. Popovitibiro, M. Lahav, L. Leiserowitz, *Acta Crystallogra. Sect. B*, 1995, **51**, 115-148.
10. A. F. Wells, *Discuss. Faraday Soc.*, 1949, **5**, 197-201.
11. Z. Berkovitch-Yellin, *J. Am. Chem. Soc*., 1985, **107**, 8239-8253.
12. R. J. Davey, B. Milisavljevic, J. R. Bourne, *J. Phys. Chem.*, 1988, **92**, 2032-2036.
13. (a) E. Vlieg, Menno Deij, Daniel Kaminski, Hugo Meekes and Willem van Enckevort, *Faraday Discuss.*, 2007, **136**, 57-69. (b) I. Weissbuch, L. Addadi, M. Lahav and L. Leiserowitz, Science, 1991, **253**, 637-645.
14. R. Kern, in *Morphology of Crystals*, ed. I. Sunagawa, Terra, Tokyo, 1987, pp 77-206.
15. J. W. Gibbs, *Collected Works, Longman*, New York, 1928.
16. (a) A. Bravais, *Etudes Cristallographiques*; Gauthier-Villars: Pasis, France, 1866. (b) G. Friedel, *Bull. Soc. Franc. Mineral*., 1907, **30**, 326-455. (c) J. D. H. Donnay and D. Harker, *Am. Mineralogist*, 1937, **22**, 446-467.
17. (a) P. Hartman, W. G. Perdok, *Acta Crystallogr*., 1955, **8**, 49-52. (b) P. Hartman, in *Crystal Growth: An Introduction*; ed. P. Hartman, North Holland, Amsterdam, 1973, Chapter 14, pp 367-402.
18. (a) P. Bennema, in *Handbook of Crystal Growth*, ed. D.T.J. Hurle, Elsevier Science Publishers, Amsterdam, 1993, Vol. 1a, Chapter 7, pp 477-581. (b) P. Hartman and P. Bennema, *J. Crystal Growth*, 1980, **49**, 145-156.
19. (a) Z. Berkovitch-Yellin, J. van Mil, L. Addadi, M. Idelson, M. Lahav, L. Leiserowitz, *J. Am. Chem. Soc*., 1985, **107**, 3111-3122. (b) M. Lahav and L. Leiserowitz, *Chem. Eng. Sci*., 2001, **56**, 2245-2253.
20. G. Clydesdale, R. B. Hammond, V. Ramachandran, K. J. Roberts, P. Mougin, *Molecular Crystals and Liquid Crystals*, 2005, **440**, 235-257.
21. (a) X. Y. Liu and P. Bennema, *Phys. Rev. B*, 1994, **49**, 765-775. (b) X. Y. Liu, E.S. Boek, W.J. Briels and P. Bennema, *Nature*, 1995**, 374**, 342-345. (c) X. Y. Liu, E.S. Boek, W.J. Briels, *J. Chem. Phys*., 1995, **103**, 3747-3754. (d) X. Y. Liu and P. Bennema, *Phys. Rev. B*, 1996, **53**, 2314-2325. (e) X. Y. Liu, *Phys. Rev. B*, 1999, **60**, 2810-2817.
22. (a) M. K. Singh, A. Banerjee and P. K. Gupta, *Cryst. Growth Des.*, 2012, **12**, 732-741. (b) M. K. Singh, A. Banerjee and P. K. Gupta, *J. Cryst. Growth*, 2012, **343**, 77-85.
23. (a) A. E. Nielsen, *Pure Appl. Chem*., 1981, **53**, 2025-2039. (b) A. E. Nielsen, *J. Crystal Growth*, 1984, **67**, 289-310.
24. C. F. Woensdregt, *Faraday Discuss*. 1993, **95**, 97-107.
25. E. S. Boek, W. J. Briels, J. van Eerden and D. Feil, *J. Chem. Phys*., 1992, **96**, 7010-7018.
26. S. Gnanasambandam and R. Rajagopalan, *CrystEngComm*, 2010, **12**, 1740-1749.
27. (a) M. Salvalaglio, T. Vetter, F. Giberti, M. Mazzotti and M. Parrinello, *J. Am. Chem. Soc.* 2012, **134**, 17221-17233. (b) M. Salvalaglio, T. Vetter, M. Mazzotti and M. Parrinello, *Angew. Chem. Int. Ed*. 2013, **52**, 13369-13372.
28. M. Salvalaglio, M. Mazzotti and M. Parrinello, *Faraday Discuss*., 2015, *179*, 291-307.
29. D. Winn and M. F. Doherty, *AIChE*, 1998, **44**, 2501-2514.
30. V. Bisker-Leib and M. F. Doherty, *Cryst. Growth Des*., 2001, **1**, 455-461.
31. M. A. Lovette and M. F. Doherty, *Cryst. Growth Des*., 2012, **12**, 656-669.
32. W. K. Burton, N. Cabrera, F. C. Frank, *Philos. Trans. R. Soc. London*, 1951, **A243**, 299-357.

33. F. C. Wireko, L. J. W. Shimon, F. Frolow, Z. Berkovitch-Yellin, M. Lahav, L. Leiserowitz, *J. Phys. Chem*,. 1987, **91**, 472–481.
34. (a) M. Hussain and J. Anwar, *J. Am. Chem. Soc*., 1999, **121**, 8583-8591. (b) S. Khoshkhoo and J. Anwar, *J. Chem. Soc. Faraday Trans*., 1996, **92**, 1023-1025.
35. I. Hod, Y. Mastai, D. D. Medina, *CrystEngComm*, 2011, **13**, 502-509.
36. C. Schmidt, C. Yürüdü, A. Wachsmuth, J. Ulrich, *CrystEngComm*, 2011, **13**, 1159-1169.
37. (a) S. Piana and J. D. Gale, *J. Am. Chem. Soc.*, 2005, **127**, 1975-1982. (b) S. Piana, M. Reyhani and J. D. Gale, *Nature*, 2005, **438**, 70-73.
38. G. Tóth, *Cryst. Growth Des.*, 2008, **8**, 3959-3964.
39. S. Piana and J. D. Gale, *J. Crystal Growth*, 2006, **294**, 46-52.
40. (a) M. K. Singh, S. K. Sharma and A. Banerjee, *CrystEngComm*, 2013, **15**, 8493-8503. (b) M. K. Singh and A. Banerjee, *Cryst. Growth Des.*, 2013, **13**, 2413-2425.
41. A. S. Myerson, in *Molecular Modelling Applications in Crystallization*, Cambridge University Press, Cambridge, 1999.
42. R. Docherty, P. Meenan, in *The Study of Molecular Materials using Computational Chemistry*, Myerson , A. S., Eds.; Cambridge University Press: Cambridge, 1999; pp. 106-165.
43. P.-O. Åstrand, A. Wallqvist, G. Karlström and P. Linse, *J. Chem. Phys*., 1991, **95**, 8419-8429.
44. (a) R. Dovesi, R. Orlando, B. Civalleri, R. Roetti, V. R. Saunders and C. M. Zicovich- Wilson, CRYSTAL: a computational tool for the ab initio study of electronic properties of crystals, *Z. Kristallogr*., 2005**, 220**, 571-573. (b) R. Dovesi, V. R. Saunders, R. Roetti, R. Orlando, C. M. Zicovich- Wilson, F. Pascale, B. Civalleri, K. Doll, N. M. Harrison, I. J. Bush, P. D'Arco, M. Llunell, CRYSTAL09 User's Manual, University of Torino, Torino, 2009.
45. S. F. Boys, F. Bernardi, *Mol. Phys*., 1970, **19**, 553-559.
46. Wolfram Koch, Max C. Holthausen, in *A Chemist's Guide to Density Functional Theory*; Wiley-VCH Press, Cambridge, MA, 1981, pp. 217-238.
47. J. F. Dobson, J. Wang, B. P. Dinte, K. McLennan, H. M. Le, *Int. J. Quantum Chem*., 2005, **101**, 579-598.
48. B. Civalleri, K. Doll and C. M. Zicovich-Wilson, *J. Phys. Chem. B*., 2007, **111**, 26-33.
49. J. D. Cox, G. Pilcher, *in Thermochemistry of Organic and Organometallic Compounds*; Academic Press, New York, 1970.
50. S. Swaminathan, B. M. Craven, R. K. McMullan, *Acta Crystallogr. Sect. B*, 1984, **40**, 300-306.
51. A. A. Chernov, *Modern Crystallography III*, Springer-Verlag: New York, 1984.
52. P. Bennema, in *Handbook of Crystal Growth*; ed. D.T.J. Hurle, Elsevier Science Publishers: Amsterdam, **1993**, Vol. 1a, Chapter 7, pp 477-581.
53. J. P. van der Eerden, in *Handbook of Crystal Growth*; ed. D.T. J. Hurle, Elsevier Science Publishers: Amsterdam, 1993; Vol. 1a, Chapter 5, pp 307−475.
54. H. Cuppen, *PhD Thesis*, Radboud University Nijmegen, The Netherlands, 2005.
55. I. Sunagawa, in *Morphology of Crystals*, ed. I. Sunagawa, Terra Scientific Publishing Com: Tokyo, 1987, Part. A, Chapter 5, pp 321-365.
56. M. F. Reedijk, J. Arsic, F. F. A. Hollander, S. A. de Vries and E. Vlieg, *Phys. Rev. Lett*., 2003, **90**, 0661031-0661034.
57. M. Ohara and R.C. Reid, *Modelling Crystal Growth Rates from Solution*; Prentice-Hill, Inc. USA, 1973, pp 59.
58. D. Aquilano, M. Rubbo, G. Mantovani, G. Sgualdino, and G. Vaccari, *J. Crystal Growth*, 1986, **74**, 10-20.
59. R. H. Fowler and E. A. Guggenheim, *Statistical Thermodynamics*, Cambridge University Press, London, 1960.
60. M. K. Singh, V. S. Tiwari, *Cryst. Growth Des.*, 2015, **15**, 3220-3234.
61. R. Docherty, K. J. Roberts, V. Saunders, *Faraday Discuss*., 1993, **95**, 11-25.
62. E. S. Boek, D. Feil, W.J. Briels and P. Bennema, *J. Crystal Growth*, 1991, **114**, 389-410.
63. Ashley R. George, Kenneth D. M. Harris, Andrew L. Rohl and David H. Gay, *J. Mater. Chem*., 1995, **5**, 133-139.
64. R. Davey, W. Fila and J. Garside, *J. Crystal Growth*, 1986, **79**, 607-613.
65. M. K. Singh and A. Banerjee, *Cryst. Res. Tech*., 2011, **46**, 1035-1043.

66. I. Weissbuch, L. Leiserowitz and M. Lahav, *Cryst. Growth Des.*, 2006, **6**, 625-628.
67. J. Anwar, J. Chatchawalsaisin and J. Kendrick, *Angew. Chem*., 2007**, 119**, 5633-5636.
68. M. K. Singh and A. Banerjee, *CrystEngComm*, 2013, **15**, 4143-4152.
69. F. H. Stillinger, *Science*, 1980, **209**, 451-457.
70. The energy correction is needed because in liquid water, each water molecule is associated with 4 hydrogen bonds. The average energy of a fully formed ice-like structure is -5.5 kcal mol^{-1}.[69] Due to the bonding of water molecules with the urea molecules at surface, only one interfacial bond is altered and remaining are unchanged. The energy needed to make this new binding is the difference between calculated $E_{s-f}^{(hkl)}$ and -1.38 kcal mol^{-1}.
71. M. Pickering, *J. Chem. Educ*., 1987, 64, 723-724.
72. (a) S.K. Sharma, Sunil Verma, B.B. Shrivastava and V.K. Wadhawan, *J. Crystal Growth*, 2002, **244**, 342-348. (b) L. N. Rashkovich and G. T. Moldazhanova, *J. Crystal Growth*, 1995, **151**, 145-152.
73. M. K. Singh *et. al*., Manuscript under preparation.

Table of contents entry only

Simulating growth morphology of urea crystals from vapour and aqueous solution

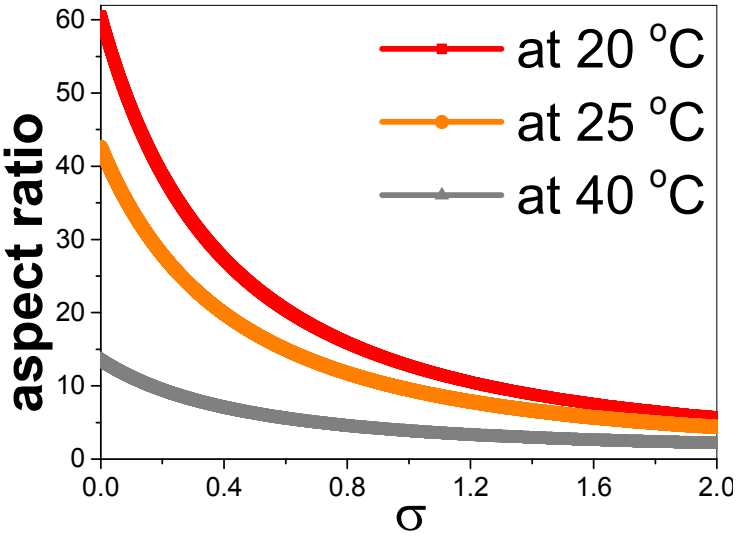

Prediction of solvent-induced crystal growth shape from its internal and interfacial atomic structure occurred due to ordering of solvent molecules has been investigated. For this purpose, a computational model has been employed to calculate growth morphologies of urea crystal from vapour and aqueous solution as function of supersaturation. Predicted growth shapes of urea crystal are in excellent agreement with experimental observations.